

# Practical Optimization of EMI Reduction in Spread Spectrum Clock Generators with Application to Switching DC/DC Converters

Fabio Pareschi, *Member, IEEE*, Gianluca Setti, *Fellow, IEEE*, Riccardo Rovatti, *Fellow, IEEE*, and Giovanni Frattini

**Abstract**—We here consider the most common technique used in spread spectrum clock generators, that is the frequency modulation of a timing signal by means of a triangularly shaped waveform. As a first step, we develop a reliable mathematical model of a spectrum analyzer, which allows us to compute the power spectrum as measured by this instrument for any signal put at its input. This is particularly important when considering spread spectrum clocking methods for electromagnetic interference reduction, since international regulations impose constraints on the peak of the spectrum of interfering signals as measured by this instrument. Thanks to the developed mathematical tool, we are able to theoretically prove that the maximum peak reduction of the measured spectrum is achieved for a *well defined* frequency of the triangular driving signal. This is in contrast with what one can obtain by optimizing the theoretical power density spectrum, where the minimum interference is ideally obtained when the triangular signal has a vanishing frequency. Results are confirmed by measurements on two commercial DC/DC switching converters.

**Index Terms**—EMI reduction, Spread Spectrum Clock Generator, Spectrum analyzer, Triangular Frequency Modulation.

## I. INTRODUCTION

THE reduction of Electro-Magnetic Interference (EMI) in electronic systems is an inherent problem in all modern equipments, as evidenced by the presence of many regulations [1, 2] which link Electro-Magnetic Compatibility (EMC) with the ability to fit the interfering power spectrum level under a prescribed mask. One of the classes of circuits which is more affected by this problem is that of DC/DC switching converters, where the presence of rapidly changing high-power signals may generate severe *radiated* or *conducted* interferences within the converter itself (i.e., the EMI source) and in other nearby circuits (EMI victims) [3].

In the design of this class of circuits, some solutions to mitigate EMI problems are always adopted [4–6]. EMC regulations require that the interfering signal power spectrum fits below a predetermined mask, i.e., that its *peak level* does not exceed a given value. Therefore, precautions based on

F. Pareschi and G. Setti are with ENDIF - University of Ferrara - Via Saragat, 1 - 44122 Ferrara (ITALY)

R. Rovatti is with DIE - University of Bologna, Viale Risorgimento, 2 - 40136 Bologna (ITALY)

F. Pareschi, G. Setti, and R. Rovatti are also with ARCES - University of Bologna, Via Toffano, 2 - 40125 Bologna (ITALY)

G. Frattini is with Texas Instruments Kilby Europe Labs, Milano - Italy  
email: (fabio.pareschi, gianluca.setti)@unife.it, riccardo.rovatti@unibo.it, giovanni.frattini@ti.com

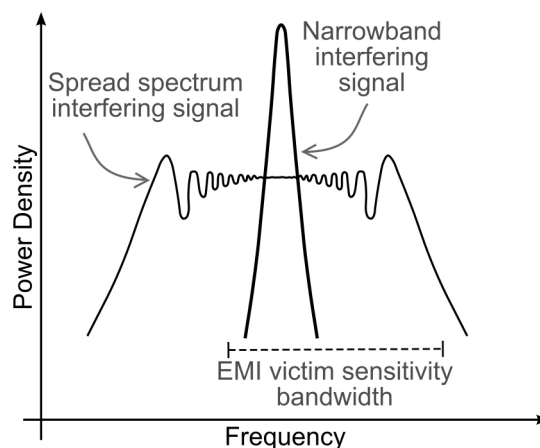


Fig. 1. When a narrow-band EMI source signal frequency matches the EMI victim sensitivity frequency, a large amount of power is transferred, with a probability of a failure in the EMI victim. Spreading the EMI source signal in a bandwidth larger than the victim sensitivity bandwidth reduces the transferred power to the victim and the probability of a failure, with an EMC improvement.

a proper layout of the circuit are frequently adopted aiming at reshaping the radiated and/or conducted power spectrum by effectively reducing its overall power. This includes using power supply filters, avoiding sharp transients by a proper snubbers design, or reducing the antenna factor by clever high-power lines routing. All these solutions are extremely efficient in the reductions of peaks at high frequencies, while the effectiveness at low frequencies may be much more limited.

We here concentrate on a different solution, first proposed in [7] and known as *dithering*, or *spread spectrum* clocking, which has attracted increasing attention in the last decade.

This technique can be applied to any synchronous DC/DC converter (i.e., to converter that synchronizes switching activities with a fixed frequency clock) as well as any other synchronous digital circuit, and can be considered as an additional and complementary EMI reduction methodology with respect to those mentioned above.

The main idea grounding this technique can be explained referring to Figure 1. To this aim, let us consider a synchronous DC/DC converter operating at steady state. In this setting, both radiated and conducted emissions have discrete narrow-band power spectra, with components at the switching frequency and its harmonics. If, by means of a Spread Spectrum Clock

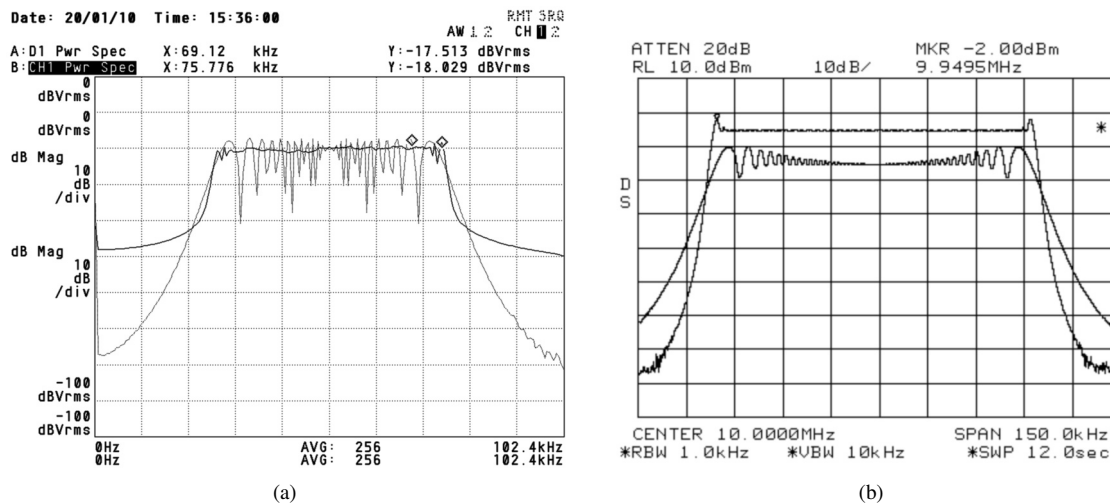


Fig. 2. Comparison between the power spectrum of a spread spectrum sinusoidal signal, measured with (a): an Agilent/HP35670A DSA; and (b): an Agilent/HP8563E analog spectrum analyzer. Two test signals have been considered, which are frequency modulated clock with a triangular driving signal, both with  $\rho = 0.02$ , and respectively with  $m = 100$  and  $m = 1000$ . The power level of the first harmonic in the unmodulated case is, respectively, 0 dBVrms and 0 dBm.

Generator (SSCG), we introduce a controlled jitter in the reference timing signal, the periodic behavior of the converter can be avoided. In this way, the conducted/radiated power spectrum is altered, and the power of any spectral component is spread over a bandwidth which depends on the jitter characteristics, thus reducing the peak of the interfering spectrum as sketched in Figure 1. Under the widely accepted assumption that EMI victims can be modeled as narrow-band filters, this technique helps reducing the transferred power in the worst case scenario, i.e., when the source emitting frequency is exactly located in one of the victim sensitivity frequency ranges, with obvious beneficial effects on the victim [8].

In recent years spread spectrum techniques have been used in many applications, ranging from class D amplifiers [9, 10] to microprocessor clock generators [7, 11–15], even to electronic ballasts [16] and LCD display panels [17]. It has been also adopted in some recent communication protocols like the Serial ATA [18–21], the Display Port [22] and the PCI Express [23]. In DC/DC switching converters this technique has been widely studied [24–31] and even applied to industrial products [32, 33] to achieve an additional EMI reduction at the cost of a very small increment of the output ripple [34].

In almost all above examples (excluding [30, 31] which employ a *period modulation*), spread spectrum clocking is achieved by means of a frequency modulation of the reference timing signal. More formally, and limiting ourselves to a simple sinusoidal signal  $s(t)$ , one has

$$s(t) = A_0 \cos \left( 2\pi f_c t + 2\pi \Delta f \int_{-\infty}^t \xi(\tau) d\tau \right) \quad (1)$$

where  $f_c$  is the carrier frequency,  $\Delta f$  is the frequency deviation and  $-1 \leq \xi(t) \leq 1$  is the normalized driving signal. The total power of this signal is  $A_0^2/2$  and it is approximately spread [35] in the Carson's bandwidth  $[f_c - \Delta f, f_c + \Delta f]$ . Roughly speaking, in a frequency modulation we are changing the instantaneous signal frequency from  $f_c - \Delta f$  (when  $\xi(t) = -1$ ) to  $f_c + \Delta f$  (when  $\xi(t) = 1$ ) linearly with  $\xi(t)$ . For a more

complex signal such as a clock or even the interfering signal radiated or conducted by a synchronous DC/DC converter it is easy to understand that changing the instantaneous frequency is equivalent to apply (1) to each harmonic, with the only difference that the  $n$ th harmonic is spread within a bandwidth of amplitude  $2m\Delta f$  [35].

Despite the fact that many different driving signals have been proposed (for example, a chaotic signal in [11, 19, 29], a pseudo-random signal in [10, 36], and an optimized patented one in [7, 13]), we will consider in this paper only the most simple and common approach in which  $\xi(t)$  is a triangular waveform with frequency  $f_m = 1/T$ . The advantage of this solution is that, assuming that both the modulation index  $m = \Delta f/f_m$  and the frequency resolution<sup>1</sup>  $R$  of the measurement instrument are large enough, the spectrum of (1), despite being actually discrete, looks continuous and approximately flat in the Carson's bandwidth. This represents the optimum behavior in terms of EMI reduction, since no peaks in the power spectrum are present.

A first aim of this paper is to reveal an important issue in most of the SSCGs' related literature when EMI measurements results are presented. In fact, regulations require that measurements are taken with an EMI receiver (that is, an analog spectrum analyzer with some additional options) and with a prescribed setting, which are, however, rarely employed in spread spectrum clocking literature (as, for example, in [17, 26]). On the contrary, quite often one computes the theoretical spectrum by means of Fourier signal analysis with a Dynamic Signal Analyzer (DSA) (as in [27, 29]). Sometimes the type of instrument used is not even specified [9, 16].

The use of the standard measuring setting prescribed by regulations is very important since the measured power spectrum is strongly dependent on it. As an example, let us consider Figure 2, which depicts the power spectrum of a frequency

<sup>1</sup> $R$  is defined as the minimum distance between two spectrum components which can be correctly resolved.

modulated sinusoidal signal<sup>2</sup> using a triangular waveform as driving signal. Figure 2(a) shows the measurements of two spectra, for  $m = 100$  and  $m = 1000$ , obtained using an Agilent/HP35670A DSA. In Figure 2(b), the same measurements are taken with an Agilent/HP8563E analog spectrum analyzer. In both instruments the normalized frequency resolution  $\rho = R/\Delta f$  has been set to 0.02 and the frequency range has been chosen to evaluate the power spectrum in the same interval in terms of normalized frequency range<sup>3</sup>  $f/\Delta f$ .

In this setting the two instruments measure the same normalized signal, so that the power spectrum shown in Figure 2(a) and in Figure 2(b) should be identical and, as highlighted in Section II, theoretically independent of  $m$ .

On the contrary, notice that the level of the power spectrum measured in Figure 2(b):

- is much higher with respect to what shown in Figure 2(a);
- depends on  $m$ . In the figure the higher the  $m$ , the larger the measured power.

The above observation gives also rise to a design problem, since a spread spectrum system should be optimized according to the spectrum measured in the EMI regulations setting and not to the theoretical one.

To approach this issue, in this paper we propose a mathematical model for the EMI receiver which allows us to compute the optimum working point for a triangular-modulation-based spread spectrum clocking system when measurements are taken with EMI regulation settings. This ensures that all efforts in designing EMC compliant systems are actually effective to pass EMC tests. Furthermore, by assuming that the behavior of EMI victims is better described by the measurement settings required by international regulation with respect to the computation of the theoretical spectrum, this would also increase the actual EMC of the designed system.

The paper is organized as follows. In Section II we compute the theoretical power spectrum of the SSCG output signal when a triangular modulation is employed, as well as its optimum working point. In Section III, we propose a mathematical model for the EMI receiver and use it to compute the spectrum of the interference measured by this instrument (the mathematical details of this derivation are reported in a separate appendix). We also show how the optimization of the EMI according to this model leads to a very different optimization point with respect to the previous case. In Section IV we show some spectrum measurements for two commercial DC/DC switching converters, while in Section V we propose some cases studies showing that the proposed optimization is not usually considered in commercial products. Finally, we draw the conclusion.

<sup>2</sup>This could be of course the first harmonic of any interfering signal.

<sup>3</sup>Note that, due to the different frequency ranges in which these two instruments can work, as it will be explained in Section II and Section III, it would be difficult to compare two measurements achieved on the same frequency range. This is the reason why we chose the setting of the instruments so that they measure the same normalized signal.

## II. THEORETICAL POWER SPECTRUM OF THE TRIANGULAR MODULATION

Let  $\xi$  be the (normalized) triangular driving signal

$$\xi(t) = \sum_k g\left(\frac{t}{T} - k\right), \quad g(\tau) = \begin{cases} 1 + 4\tau & -\frac{1}{2} < \tau \leq 0 \\ 1 - 4\tau & 0 < \tau \leq \frac{1}{2} \\ 0 & \text{elsewhere} \end{cases}$$

By using the standard signal analytical representation approach [37], the modulated tone in Equation (1) can be rewritten as

$$s(t) = A_0 \operatorname{Re} \left( e^{j2\pi(f_c t + \Delta f \int_{-\infty}^t \xi(\tau) d\tau)} \right) = \operatorname{Re} \left( e^{j2\pi f_c t} \tilde{s}(t) \right) \quad (2)$$

where the complex envelope  $\tilde{s}(t)$  is implicitly defined. The link between the (bilateral) power spectrum  $S(f)$  of  $s(t)$  and the base-band power spectrum  $S_B(f)$  of  $\tilde{s}(t)$  is

$$S(f) = \frac{1}{4} S_B(f - f_c) + \frac{1}{4} S_B(-f - f_c) \quad (3)$$

so that the analysis of  $\tilde{s}(t)$  is enough to characterize  $S(f)$ . Note that the total power of  $\tilde{s}(t)$  is  $A_0^2$ , that is also the peak level of  $S_B(f)$  when considering the unmodulated case, for which  $\tilde{s}(t) = A_0$ .

By defining

$$G(\tau) = \int_{-\infty}^{\tau} g(\zeta) d\zeta = \begin{cases} (1 + 2\tau)\tau & -\frac{1}{2} < \tau \leq 0 \\ (1 - 2\tau)\tau & 0 < \tau \leq \frac{1}{2} \\ 0 & \text{elsewhere} \end{cases}$$

$\tilde{s}(t)$  can be rewritten as

$$\tilde{s}(t) = A_0 e^{j2\pi \Delta f T \sum_k G(\frac{t}{T} - k)} = A_0 e^{j2\pi m \sum_k G(\frac{t}{T} - k)} \quad (4)$$

i.e.,  $\tilde{s}(t)$  is periodic with period  $T$ , and can be expressed as the complex Fourier series

$$\tilde{s}(t) = \sum_{k=-\infty}^{\infty} c_k e^{\frac{j2\pi k t}{T}}$$

where coefficients  $c_k$  are real, and given by

$$\begin{aligned} c_k &= \frac{A_0}{T} \int_{-\frac{T}{2}}^{\frac{T}{2}} e^{-j2\pi k \frac{t}{T}} \tilde{s}(t) dt = \\ &= A_0 \int_{-1/2}^0 e^{-j2\pi k \tau} e^{j2\pi m(1+2\tau)\tau} d\tau + \\ &+ A_0 \int_0^{1/2} e^{-j2\pi k \tau} e^{j2\pi m(1-2\tau)\tau} d\tau \end{aligned} \quad (5)$$

The above integrals can be easily computed in a closed form using the error function and its complementary over the complex number set. Furthermore, by recalling the relation between these functions and the Fresnel functions [38], we can express (5) as

$$\begin{aligned} c_k &= \frac{A_0}{\sqrt{2m}} \cos\left(\frac{\pi(m-k)^2}{4m}\right) \left( C\left(\frac{m-k}{\sqrt{2m}}\right) + C\left(\frac{m+k}{\sqrt{2m}}\right) \right) + \\ &+ \frac{A_0}{\sqrt{2m}} \sin\left(\frac{\pi(m-k)^2}{4m}\right) \left( S\left(\frac{m-k}{\sqrt{2m}}\right) + S\left(\frac{m+k}{\sqrt{2m}}\right) \right) \end{aligned}$$

where  $C$  and  $S$  are respectively the FresnelC and FresnelS functions. Therefore,  $S_B(f)$  is discrete, with components of power  $c_k^2$  at frequencies  $\pm k/T$ , that is

$$S_B(f) = \sum_{k=-\infty}^{\infty} c_k^2 \delta\left(f - \frac{k}{T}\right) \quad (6)$$

where  $\delta$  is the classical Dirac's distribution.

The expression (6) needs to be used in (3) to get the actual signal power spectrum, which has to be compared with the ones measured with a DSA and shown in Figure 2(a).

Before doing so, some consideration are in order. The DSA is based on the Discrete Fourier Transform (DFT) of the sampled input signal [39], which makes it capable of measuring a spectrum that is very similar to the theoretical one. Yet, unfortunately, the requirement of an high-precision sampling makes the instrument able to correctly operate only on very low frequency signals. Furthermore, the exact measurement of  $S_B(f)$  is possible only when the instrument resolution  $R$  is vanishing. If this condition does not hold the instrument measures only an approximation  $S'_B(f)$  of  $S_B(f)$ , which even appears as a continuous spectrum when  $R$  is larger than the distance between two consecutive spectral components of the input signal, i.e., if  $R > 1/T$  or  $\rho > 1/m$ .

This is confirmed by the measurements shown in Figure 2(a), for which the sampling frequency is 204.8 kHz, the frequency deviation  $\Delta f$  is 25 kHz, the number of lines (i.e. points in the DFT) is 400, so that  $R = 512$  Hz and  $\rho \approx 0.02$ . As it can be seen, for  $m = 100$ , the harmonics present in (6) are still partially identifiable, while for  $m = 1000$  the measured spectrum appears to be continuous.

More formally, let us define with  $H(f)$  the normalized measuring low-pass filter (i.e., with pass-band  $-1/2 < f < 1/2$ ) so that  $S'_B(f)$  is given by the discrete convolution

$$\begin{aligned} S'_B(f) &= S_B(f) * H(f/R) = \sum_{k=-\infty}^{\infty} c_k^2 \left| H\left(\frac{k/T-f}{R}\right) \right|^2 \\ &= \sum_{k=-\infty}^{\infty} c_k^2 \left| H\left(\frac{k/m-f/\Delta f}{\rho}\right) \right|^2 \end{aligned} \quad (7)$$

which depends only on  $m$ , on the normalized resolution  $\rho$  defined as  $R/\Delta f$ , and on the normalized frequency  $\rho = f/\Delta f$ . By using  $m$  and  $\rho$  as in Figure 2 and a Gaussian shaped  $H(f)$ , we get the normalized spectra drawn in Figure 3. These spectra match very well with the corresponding ones in Figure 2(a).

The peak level of the power spectrum measured with the DSA is given by the function  $\max_f S'_B(f)$ , an example of which has been depicted in Figure 4 as a function of  $m$  for a few values of  $\rho$ . As already suggested by Figure 2(a) and 3, the peak level reduction increases with  $m$  up to a saturation level which depends on  $\rho$ . Note that this curve is similar to the one presented in [26], where the saturation effect due to the finite normalized resolution  $\rho$  was not considered.

Interestingly enough, the saturation level reached in Figure 4 can be easily computed under the simplifying assumption of a measuring filter  $H(f)$  with rectangular shape. In this case, when computing  $S'_B(f)$  as in (7), we have a non-vanishing contribution only from the spectral components such that

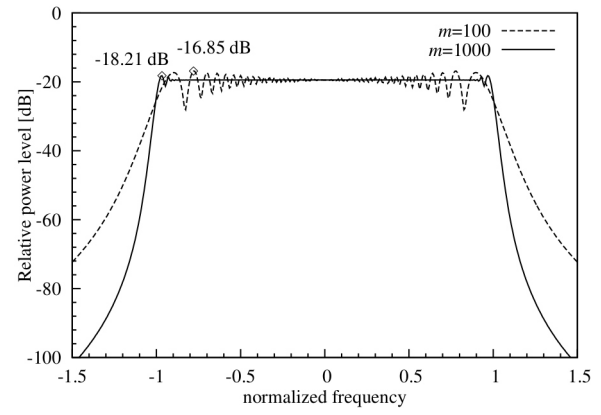


Fig. 3. Normalized spectrum  $S'_B(f/\Delta f)/A_0^2$  according to the theoretical power spectrum measured with a finite resolution, plotted for  $m = 100$  and for  $m = 1000$ , and by setting a normalized resolution  $\rho = 0.02$ . These parameters are the same used in Figure 2.

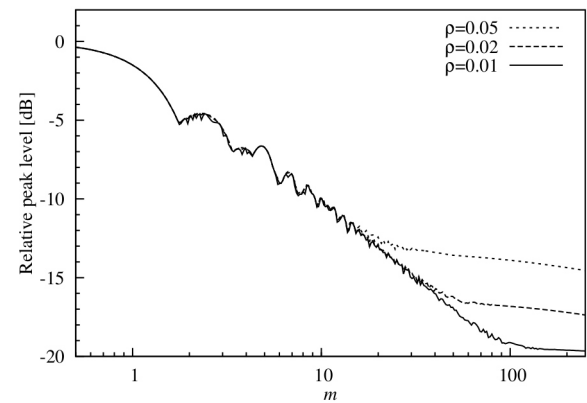


Fig. 4. Relative peak level of the power spectrum of a triangular modulation (the 0 dB reference level is the unmodulated case) according to the theoretical power spectrum computed in (7). In accordance with the empirical observations of Figure 2, the EMI reduction increases with  $m$ , up to the saturation level  $10 \log(\rho/2)$ .

$|\frac{k/T-f}{R}| < \frac{1}{2}$ , i.e.,  $|k - m \frac{f}{\Delta f}| < m \frac{\rho}{2}$ . Saturation occurs when the number  $m\rho$  of these components is large enough. Furthermore, we consider the additional simplifying assumptions of a flat spectrum in the Carson's bandwidth and vanishing outside it. In this setting, the value of the coefficients  $c_k$  can be computed considering that in the bandwidth  $[-\Delta f, \Delta f]$  there are  $2m$  spectral lines, each equally spaced by  $f_m$ , and that  $\sum_k c_k^2 = A_0^2$ . The actual value of each  $c_k^2$  coefficient depend on  $k$ , but, using the first assumption, since the spectral components are estimated through an (averaging) measuring filter, when  $m\rho$  is large enough, we may replace the actual value of  $c_k^2$  with its average value  $\bar{c}_k^2 = A_0^2/(2m)$  for  $|k| < m$  and 0 otherwise. With this (7) becomes:

$$\begin{aligned} S'_B(f) &\approx \sum_{k=-m}^m \bar{c}_k^2 \left| H\left(\frac{k/m-f/\Delta f}{\rho}\right) \right|^2 \approx \\ &\approx \sum_{k=m \frac{f}{\Delta f} - m \frac{\rho}{2}}^{m \frac{f}{\Delta f} + m \frac{\rho}{2}} \bar{c}_k^2 \approx \frac{A_0^2}{2m} m\rho = A_0^2 \frac{\rho}{2} \end{aligned}$$

This value is in perfect agreement with the one observed both

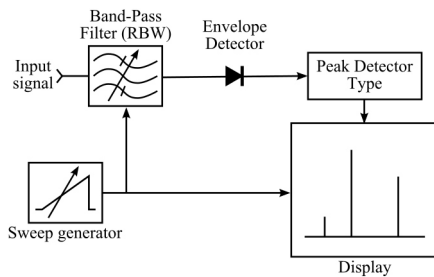


Fig. 5. Sweeping filter model for a spectrum analyzer

in Figure 3 and in Figure 4.

### III. EMI-RECEIVER BASED POWER SPECTRUM OF THE TRIANGULAR MODULATION

Despite its theoretical interest, the curve of Figure 4 is not the correct tool to achieve optimal EMI reduction since all regulations require that measurements are performed with an EMI receiver instead of a DSA.

To cope with this, we need to obtain an optimization curve based on the actual EMI receiver measurements. To do so, let us refer to the simplified model of the spectrum analyzer shown in Figure 5.

The core of the instrument is a tunable band-pass filter whose bandwidth represents the resolution  $R$  of the receiver (and is therefore called the Resolution Bandwidth – RBW – of the instrument) whose center frequency is  $f_0$  and whose transfer function can be expressed as  $H\left(\frac{f-f_0}{R}\right) + H\left(\frac{-f-f_0}{R}\right)$ . The value  $S'(f_0)$  of the measured power spectrum of the input signal at the generic frequency  $f_0$  is achieved by tuning the RBW filter central frequency to it and by measuring the power of the filtered signal. More specifically, the filtered signal is demodulated by an envelope detector and then analyzed by the so-called *peak* detector, which performs the actual power estimation. The central frequency  $f_0$  is slowly and continuously moved, by means of a sweep signal generator, to analyze all the frequencies in the range of interest. This approach is known as *sweeping filter*.

To derive the mathematical model of the instrument, let us assume that  $f_0$  is constant so that we can consider the system as time-invariant. Let us indicate with  $s_H(t)$  the signal filtered by the RBW filter, and with  $\tilde{s}_H(t)$  its analytical representation. An ideal envelope detector extracts the absolute value  $|\tilde{s}_H(t)|$ , and the peak detector estimates the signal power from this function. For the sake of simplicity we consider the *positive peak detector*, which computes  $S'(f_0)$  as the power of a sinusoidal signal whose amplitude is equal to the maximum observed value of  $\tilde{s}_H(t)$ , i.e., referring to a bilateral spectrum

$$S'(f_0) = S'(-f_0) = \frac{\max_t |\tilde{s}_H(t)|^2}{4}$$

In order to use a notation similar to the previous case, let us introduce the spectrum  $S'_B(f_0)$  such that  $S'_B(\tilde{f}_0) = S'_B(f_0 - f_c) = \max_t |\tilde{s}_H(t)|^2$ . This spectrum, for which an equation in the form of (3) still holds, can be directly compared to the base-band spectrum computed in Section II.

Note that the proposed model has two small differences with respect to a real spectrum analyzer. First, since high-quality tunable filters are very difficult to realize, hardware implementations are based on a frequency translation of the input signal similarly to what happens in a superheterodyne receiver (*sweeping signal* approach). This has however no effect on our considerations, since the high-level model of the system remains the same. Second, EMC regulations allow the use of both the positive peak detector and of the *quasi-peak detector*, which is designed to make an intermitting disturbance signal more tolerable than a fixed one. However, the latter detector is strongly non-linear and we will not consider its possible adoption in our model, since it would make the analytic analysis intractable without substantially altering the main result we will achieve.

Based on the above considerations,  $S'_B(\tilde{f}_0)$  can be obtained using a closed form expression for  $\tilde{s}_H(t)$ , which has to be computed as the convolution between the analytical representation  $\tilde{s}(t)$  of the input signal  $s(t)$  and the impulse response  $h_B(t)$  of the base-band equivalent of the RBW filter, whose transfer function is given by  $H_B(\tilde{f}_0) = H\left(\frac{f-\tilde{f}_0}{R}\right)$ .

Let us consider the typical four-pole, nearly-Gaussian-shape filter used in Agilent/HP Spectrum Analyzers [40], for which

$$|H(f)|^2 = \frac{1}{\left(1 + (f/\nu_0)^2\right)^4} \quad (8)$$

where  $\nu_0 = \frac{1}{2\sqrt{2^{1/4}-1}}$  to ensure that the cut-off frequency according to a  $-3$  dB definition is  $1/2$ , i.e.,  $|H(\pm 1/2)|^2 = 1/2$ . Since the filter transfer function satisfies the non-distortion conditions, we may assume without loss of generality that  $H(f)$  is real so that the impulse response of the base-band filter can be computed as

$$h_B(t) = \frac{\pi\nu_0 R}{2} e^{j2\pi\tilde{f}_0 t} e^{-2\pi\nu_0 R|t|} (1 + 2\pi\nu_0 R|t|) \quad (9)$$

In this way

$$\tilde{s}_H(t) = \int_{-\infty}^{\infty} \tilde{s}(\tau) h_B(t - \tau) d\tau$$

that, using (4) and (9), can be expressed using the normalized function  $\tilde{s}_N(\tau) = \tilde{s}_H(\tau T)$  which depends only on  $\tau = t/T$  and on the parameters  $m$ ,  $\rho$  and  $\tilde{f}_0/\Delta f$ , and whose expression is reported in Appendix A.

Hence, one can obtain the measured spectrum by recalling that

$$S'_B(\tilde{f}_0) = \max_t |\tilde{s}_H(t)| = \max_{\tau} |\tilde{s}_N(\tau)| \quad (10)$$

Despite cumbersome and quite complex, the achieved expression for  $S'_B(\tilde{f}_0)$  can be easily evaluated numerically to achieve spectra that can be compared with the ones of Figure 2(b), measured with  $R = 1$  kHz and  $\Delta f = 50$  kHz, i.e.,  $\rho = 0.02$ . Plugging these parameters in (10) we get the two spectra of Figure 6, which are in perfect agreement with the measured ones.

As in the previous case, we can numerically evaluate the function  $\max_{\tilde{f}_0} S'_B(\tilde{f}_0)$  to obtain an optimization curve to maximize EMC when interference is measured using an EMI

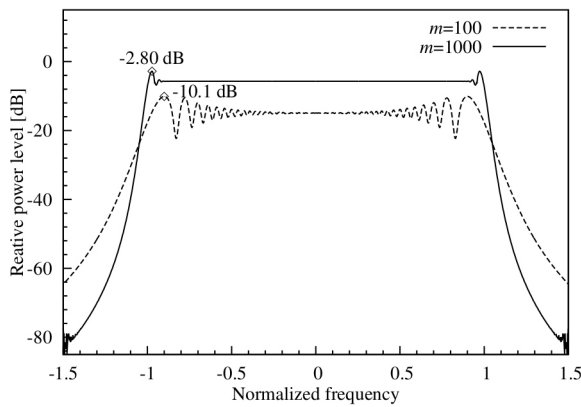


Fig. 6. Normalized spectrum  $S'_B(f/\Delta f)/A_0^2$  computed according to the proposed EMI receiver model, plotted for  $\rho = 0.02$ ,  $m = 100$  and for  $\rho = 0.02$ ,  $m = 1000$ . These parameters are the same used in Figure 2.

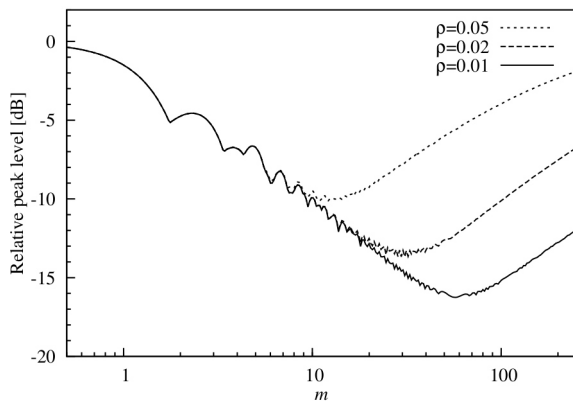


Fig. 7. Peak level (the 0 dB reference level is the unmodulated case) of the triangular modulation power spectrum according to proposed EMI receiver model.

receiver. Results can be seen in Figure 7, and show that the EMI reduction does not increase monotonically with  $m$ . Rather, there is an optimum value of  $m$  for which maximum EMI reduction is achieved. For larger values of  $m$ , the EMI reduction decreases to 0 dB, that is, *no reduction is achieved with respect to the unmodulated case*. This corresponds to the intuition that, assuming a very slow driving signal (i.e.,  $T$  long and  $m$  high), the modulated signal appears to be very similar to a single tone to the instruments, which consequently estimates its power as the one of an unmodulated sinusoid. Note that this is in accordance with the plots reported in Figures 2 and 6 which show an increase of the spectrum peak level for increasing values of  $m$ .

#### IV. APPLICATION OF THE TRIANGULAR MODULATION TO DC/DC SWITCHING CONVERTERS

The aim of this section is to apply to synchronous DC/DC switching converters the procedure developed so far for the EMI optimization according to measurements taken with an analog spectrum analyzer. As shown in the following, independently of the converter architecture, when applying a spread spectrum to the reference clock controlling the Pulse Width Modulation (PWM) signal generator, we are changing

the instantaneous frequency of all components in the power spectrum of any internal and potentially interfering signal thus modulating them as discussed in the previous sections.

Note also that some parameters in DC/DC switching converters are actually fixed by design constraints, and cannot be used for the proposed optimization. For example, the maximum instantaneous switching frequency  $f_c + \Delta f$  may be set by the speed of the switches, or possibly by a bound on the converter efficiency. Similarly, the lower instantaneous frequency  $f_c - \Delta f$  could be set by a constraint on the output ripple. These constraints usually fix the value of  $\Delta f$ . Furthermore, the instrument resolution  $R$  is set by standard regulations. Conversely, the value of  $f_m$  does not usually suffer from similar constraints and can be considered a degree of freedom to be used to optimize the EMI reduction in the system. If we also consider that varying  $f_m$  has a negligible impact on other converter performance such as ripple [34], the EMI reduction optimization based on the proper tuning of  $f_m$  can be considered extremely appealing.

In the following we present two case studies among commercially available DC/DC switching converters. Assuming that circuitual constraints fix the value for  $\Delta f$  and that  $R$  is given by regulations, we will look for the  $f_m$  value that optimizes EMI reduction according to our theoretical model, and we will verify this by direct measurements. From a mathematical point of view, this is equivalent to fix the  $\rho$  value and look for the optimum value of  $m$ . Of course, since each harmonic of the radiated or conducted power spectrum presents different  $m$  and  $\rho$  indexes, the optimum EMI reduction can be guaranteed for a single harmonic only. We will focus on the first one, which is typically the harmonic with the largest power and the highest probability to cause a failure in a victim.

The first case study is the TI LM3424 evaluation board [41]. This board embeds a PWM controller specifically designed for LED drivers, i.e., it has a constant output current (more precisely, 1 A output), a quite large ripple (about 100 mV) and it is designed in a boost configuration. During measurement, this board has been loaded by a 22  $\Omega$  power resistor. The second one is a TI LM5088-1 evaluation board [32], which is constructed to achieve a constant output voltage of 5 V for generic applications. The board is designed as a buck converter, and the ripple is quite limited (about 10 mV). During measurement, this board has been loaded by a 15 W light bulb.

Both boards accept a synchronization input signal. This feature has been exploited to introduce spread spectrum, driving the boards with an Agilent/HP33220A arbitrary function generator implementing a triangular-based frequency modulated clock. The reason why we show measurements on these two boards is to prove the generality of our approach. The two boards in fact embed two DC/DC controllers which are almost completely different in topology (boost vs buck), in the feedback control loop (current feedback for constant output current vs voltage feedback for constant output voltage) and in target application (application specific – LED – vs generic). However, in both boards EMI measurements fit very well with expected results.

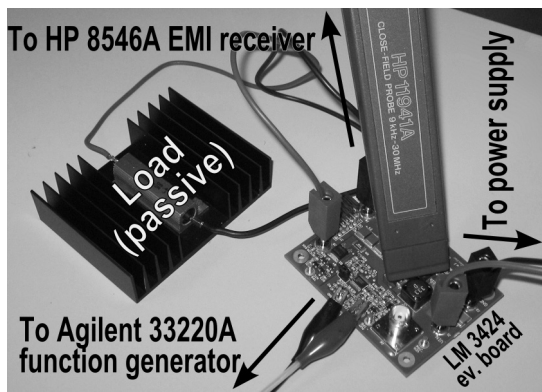


Fig. 8. Measurements setup for the LM3424 evaluation board, showing the board itself, the passive load and the HP11941A close-field probe. The close-field probe is directly connected with a  $50\Omega$  cable to the HP8546A EMI receiver.

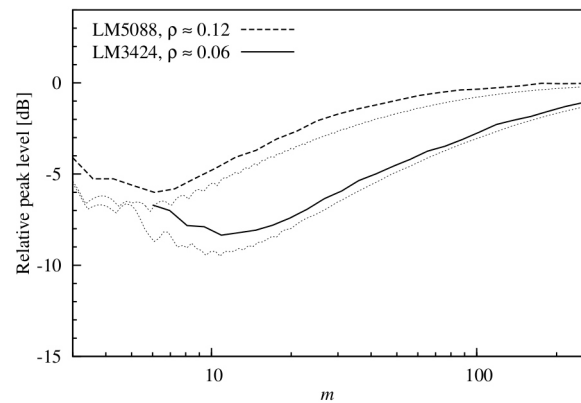
Emissions from the boards have been measured by means of an HP11941A close-field probe, connected to an HP8546A, which is a spectrum analyzer certified for EMI measurements. The close-field probe has been placed in proximity of the board inductor, which turned out to be the major source of electromagnetic radiations. As an example, the EMI measurement setup for the LM3424 is shown in Figure 8.

For the first board, we have set  $f_c = 1$  MHz and  $\Delta f = 100$  kHz, while for the second  $f_c = 500$  kHz and  $\Delta f = 50$  kHz. According to regulations [3], for frequencies in this range the 9 kHz EMI filter must be selected on the EMI receiver. Since EMI filters are defined in terms of their  $-6$  dB bandwidth, and assuming a four-pole nearly Gaussian shape also in this case, Equation (8) can still be applied by setting  $\nu_0 = \frac{1}{2\sqrt{2^{1/2}-1}}$ , which results in a  $-3$  dB bandwidth of approximately 6.08 kHz.

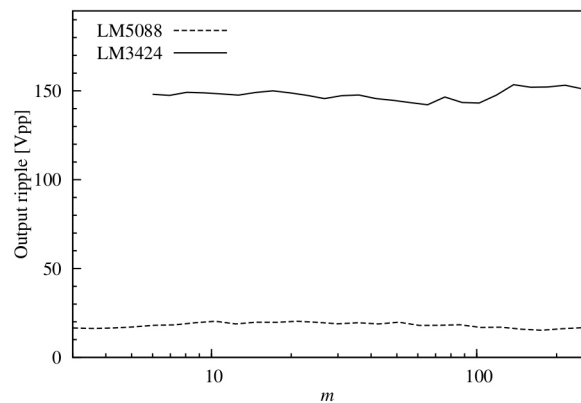
By considering this adjustment, we get  $\rho \approx 0.06$  for the first case and  $\rho \approx 0.12$  for the second one. By looking at the optimization curves for these values, the optimum value for  $m$  is around 10 with an EMI reduction around 9 dB in the first case, and an optimum value for  $m$  around 6 in the second one, with an expected EMI reduction of 7 dB. The achieved optimum  $m$  value corresponds to a triangular driving frequency which is in both cases around 8 kHz.

Figure 9(a) shows the theoretical optimization curve and the measured one for the two considered converters. The measured curve approximates very well the theoretical one in the two cases, and both the optimum  $m$  value and the expected EMI reduction are confirmed by measurements. We want to stress that this optimization is achieved at no cost for other converter parameters. As an example, we show in Figure 9(b) how the output ripple is affected by changing  $m$  value (i.e., by changing  $f_m$  value). As it can be seen, in both cases the ripple is almost constant for all the considered range.

Finally, we show two detailed measurements, one for each converter. Figure 10 shows the comparison between the measured power spectrum in the neighborhood of the switching frequency in the unmodulated case (i.e., with spread spectrum disabled) and the triangular modulated one with the optimum modulation frequency  $f_m = 8$  kHz for the LM3424 board. As



(a)



(b)

Fig. 9. (a): comparison between the theoretically expected EMI reduction for the two considered DC/DC switching converters (dotted lines) and the measured one for different values of  $m$ ; and (b) measured ripple for the two converters for different values of  $m$ . Measurements for  $m < 3$  (LM5088) or  $m < 6$  (LM3424) are not taken due to limitations in the Agilent 33220A generator.

it can be seen, the measured EMI reduction is 8.4 dB, which is in very good agreement with the theoretical expectation. Figure 11 shows the output ripple measured in the LM5088 board for three different  $f_m$  frequencies. Very small changes between the three cases can be observed, thus experimentally confirming the very weak dependence on  $f_m$  of the output ripple.

## V. CASE STUDY FOR THE TRIANGULAR MODULATION

All major semiconductor companies commercialize several spread-spectrum clock generators. In the majority of the cases many spreading parameters are not explicitly mentioned, making it impossible to perform a comprehensive comparison of their EMI reduction performance. Yet, we are able to show that several of them could benefit of the parameter optimization procedure developed in this paper.

As a first example, let us take the already considered LM5088-1 by Texas Instruments. This PWM controller features a built-in  $\pm 5\%$  frequency dithering function though an internally generated triangular signal to reduce the conducted and radiated EMI. Despite the fact that modulation parameters can be set in a wide range, from direct measurements on

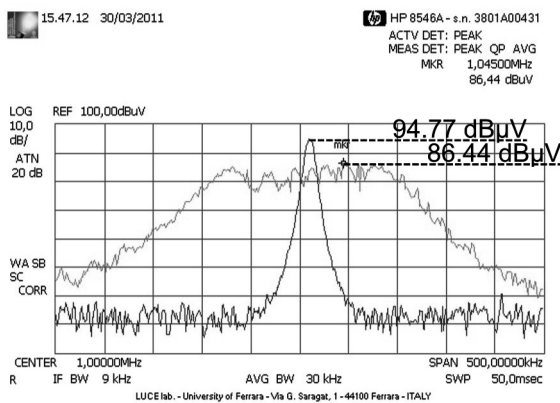


Fig. 10. Comparison between emitted power spectrum for the LM3424 evaluation board when spread spectrum is disabled, and when using a triangular spread spectrum with the optimum modulation index  $m \approx 12.5$ .

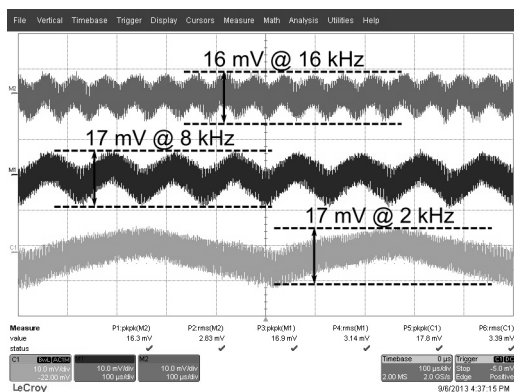


Fig. 11. Ripple measurements for the LM5088 evaluation board, at three different values of triangular driving signal frequency  $f_m$ .

a LM5088 Evaluation Board [32], we got  $f_c \approx 250$  kHz,  $\Delta f \approx 8$  kHz and  $T \approx 550$   $\mu$ s (i.e.,  $m \approx 4.5$ ). For this operating frequency, regulations require to use  $R = 9$  kHz so (considering the RBW filter correction factor)  $\rho \approx 0.74$ . Figure 12 shows (upper trace, solid line) the optimization curve for this set of parameters and the circuit operating point in the parameter space, from which one can immediately achieve that the measured EMI reduction is very small in this particular setting. On the contrary, by using  $m \approx 1.5$  one would get an approximately 2.5 dB additional EMI reduction.

ON Semiconductors offers P6P82PS01A, a companion IC that can be dropped-in on to the frequency control node in a PWM controller to introduce spread spectrum. In the case study presented in the datasheet [33] and based on the TPS54317 evaluation board clocked at 1 MHz, test settings include a  $\pm 20\%$  spreading (i.e.,  $\Delta f = 200$  kHz),  $f_m = 25$  kHz and, even if not explicitly indicated, we can assume  $R = 9$  kHz. According to this, we get  $\rho \approx 0.03$  and  $m = 8$ , so that we expect an EMI reduction of approximately 8 dB (see point P6P82PS01A in Figure 12), that is very similar to the one measured by ON and indicated in [33] for the first harmonic. By increasing the modulation index to  $m \approx 11$ , we would get an approximately 5.5 dB additional EMI reduction.

Extending this survey also to SSCGs not specifically de-

signed for DC/DC converter applications, many commercial products may also be considered. For basically all of them, very few data on the modulation parameters are available in the datasheets. Moreover, the common criterion when designing a triangular or periodic modulation based SSCG is to fix the triangular frequency  $f_m$  just outside the audible frequency range.

For example, all Cypress devices employ a particular patented modulation known as Hershey-Kiss modulation [13], which is quite similar to the triangular one, and whose performances in terms of EMI reduction are slightly better than the ones given by a triangular profile, but for which we can assume that the analysis in Section III still holds. If we look at the example in the CY25561 datasheet [14], we can find a typical application employing a 65 MHz clock generator with a 3.1% spreading (i.e.,  $\Delta f \approx 1$  MHz). For such a frequency, the 120 KHz EMI filter must be used to measure the spectrum, which is equivalent to a 81 kHz standard RBW filter. In this case  $\rho \approx 0.075$ . The frequency of the driving signal is 27.9 KHz, i.e.,  $m \approx 35$ . According to the datasheet, the EMI reduction is measured in 5.48 dB, which is approximately the same value we can find in the corresponding optimization curve of Figure 12 computed for the triangular modulation (point CY25561). Reducing  $m$  to a value between 6 and 10 (which still ensures that  $f_m$  is out of the audible bandwidth) would result in an increase of the EMI reduction by additional 3 dB.

For the Fujitsu MB88155 [15], a typical configuration is with the main output frequency equal to 66 MHz with a 2% spreading, i.e.,  $\Delta f = 660$  KHz. For these settings,  $\rho \approx 0.123$ . The triangular driving signal frequency is 32.4 kHz, so that  $m \approx 20$ . According to the corresponding optimization curve in Figure 12 (see point MB88155), by reducing  $m$  to approximately 4 one can gain almost 5 dB in EMI reduction.

Spread spectrum techniques are also allowed in some data transmission protocols, where all modulation parameters are fixed and standardized in order to ensure that all devices connected can tolerate the introduced dithering.

An example is the SATA protocol [18] where, according to specifications, the triangular modulation period  $T$  should lay between 30  $\mu$ s and 33  $\mu$ s, the allowed spreading bandwidth is 0.5% of the carrier frequency  $f_c \in \{1.5$  GHz, 3 GHz $\}$ . For these frequencies, the 120 kHz RBW filter must be used. In the first case,  $m \approx 120$  and  $\rho \approx 0.0216$  (see point SATA-1.5GHz in Figure 12). By decreasing  $m$  to approximately 30 it is possible to get 4 additional dB in EMI reduction. In the second case,  $m \approx 235$  and  $\rho \approx 0.0108$  (see point SATA-3GHz). By decreasing  $m$  to approximately 55 it is possible to get an additional 4.5 dB EMI Reduction.

Also the DisplayPort standard [22] allows spreading techniques, with  $T$  in the range 30 – 33  $\mu$ s, and a spreading bandwidth equal to 0.5% of the carrier. The carrier frequency is set to 2.7 GHz for the high-speed link, and 1.62 GHz for low-speed link. In the first case,  $m \approx 220$  and  $\rho \approx 0.012$  (point DP-fast); however a value of  $m$  around 55 allows almost 5 additional dB in EMI Reduction. In the second case,  $m \approx 130$  and  $\rho \approx 0.02$  (point DP-slow), and the EMI reduction can be improved by 4 dB decreasing  $m$  to about 20.

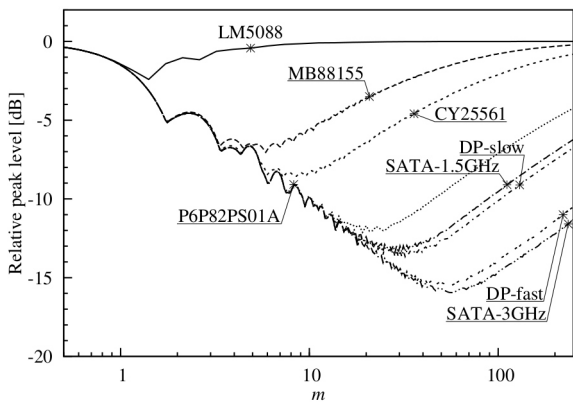


Fig. 12. Optimization curves and working points for the case study examples considered in Section V.

## VI. CONCLUSION

In this paper we consider the frequency modulation of a clock by means of a triangular shaped driving signal, since this is one of the most common technique used in spread spectrum clock generators. After the introduction of a mathematical model of the DSA and EMI receiver, we are able to compute the power spectrum measured with these two instruments from the knowledge of the theoretical power density spectrum.

This allows a *practical* optimization of EMI reductions, i.e. an optimization which is based on the measurement setup required by regulations. Here the spectrum must be measured with an EMI receiver, for which the optimization is achieved for a well defined value of the modulation index  $m$ . This is in contrast with the classical optimization based on the theoretical power spectrum density or on the DSA measurements which leads to the completely different conclusion that reduction simply increases with the value of  $m$ .

Measurements on two DC/DC switching converter evaluation boards with spread spectrum capabilities confirm the validity and the potential for practical applications of the developed mathematical framework.

## APPENDIX A

### COMPUTATION OF $\tilde{s}_N(\tau)$

Let us define the normalized function  $\tilde{s}_N(\tau)$  as

$$\begin{aligned} \tilde{s}_N(\tau) &= \int_{-\infty}^{\infty} \tilde{s}(T\zeta) T h_B(T\tau - T\zeta) d\zeta = \\ &= \int_{-\infty}^{\infty} A_0 e^{j2\pi m \sum_k G(\zeta-k)} \frac{\pi \nu_0 m \rho}{2} e^{j2\pi \frac{\tilde{f}_0}{\Delta f} (\tau-\zeta)} \cdot e^{-2\pi \nu_0 m \rho |\tau-\zeta|} (1 + 2\pi \nu_0 m \rho |\tau - \zeta|) d\zeta \end{aligned}$$

To simplify the computation, let us introduce

$$\tilde{s}s(\tau) = \begin{cases} A_0 e^{j2\pi m G(\tau)} & -\frac{1}{2} < \tau < \frac{1}{2} \\ 0 & \text{otherwise} \end{cases}$$

$$\tilde{s}s_N(\tau) = \int_{-\frac{1}{2}}^{\frac{1}{2}} \tilde{s}s(\zeta) T h_B(T\tau - T\zeta) d\zeta$$

With this,  $\tilde{s}_N(\tau) = \sum_k \tilde{s}s_N(\tau - k)$ . To obtain a closed form expression, one may first observe that the first kind singularity

of  $G(\tau)$  for  $\tau = 0$  can be circumvented by splitting the interval  $[-\frac{1}{2}, \frac{1}{2}]$  into two equal parts so that:

$$\begin{aligned} \tilde{s}s_N(\tau) &= A_0 \frac{\pi \nu_0 m \rho}{2} \left( \tilde{s}s_N^{(l)}(\tau) + \tilde{s}s_N^{(r)}(\tau) \right) \\ \tilde{s}s_N^{(l)}(\tau) &= \int_{-\frac{1}{2}}^0 e^{j2\pi m (1+2\zeta)\zeta} e^{j2\pi m \frac{\tilde{f}_0}{\Delta f} (\tau-\zeta) - 2\pi \nu_0 m \rho |\tau-\zeta|} \cdot (1 + 2\pi \nu_0 m \rho |t - \zeta|) d\zeta \\ \tilde{s}s_N^{(r)}(\tau) &= \int_0^{\frac{1}{2}} e^{j2\pi m (1-2\zeta)\zeta} e^{j2\pi m \frac{\tilde{f}_0}{\Delta f} (\tau-\zeta) - 2\pi \nu_0 m \rho |\tau-\zeta|} \cdot (1 + 2\pi \nu_0 m \rho |t - \zeta|) d\zeta \end{aligned} \quad (11)$$

Furthermore, since  $\zeta \in [-\frac{1}{2}, 0]$  in  $\tilde{s}s_N^{(l)}(\tau)$  ( $\zeta \in [0, \frac{1}{2}]$  in  $\tilde{s}s_N^{(r)}(\tau)$ ) the corresponding integral expressions in (11) can be split into different sub-integrals considering the three cases  $\tau < -1/2$  ( $\tau < 0$ ),  $-1/2 < \tau < 0$  ( $0 < \tau < 1/2$ ) and  $\tau > 0$  ( $\tau > 1/2$ ) respectively. By introducing the two constants  $k_1 \in \{-1, 1\}$  and  $k_2 \in \{-\nu_0 m \rho, \nu_0 m \rho\}$ , and defining the three auxiliary functions

$$\begin{aligned} \Phi_1(\tau; k_2, \phi_2, \phi_3) &= e^{j2\pi m \frac{\tilde{f}_0}{\Delta f} \tau - 2\pi k_2 \tau} ((1 + 2\pi k_2 \tau) \phi_2 + 2\pi k_2 \phi_3) \\ \Phi_2(\tau_1, \tau_2, k_1, k_2) &= \int_{\tau_1}^{\tau_2} e^{j2\pi m (1-2k_1\zeta)\zeta} e^{-j2\pi m \frac{\tilde{f}_0}{\Delta f} \zeta + 2\pi k_2 \zeta} d\zeta \\ \Phi_3(\tau_1, \tau_2, k_1, k_2) &= \int_{\tau_1}^{\tau_2} e^{j2\pi m (1-2k_1\zeta)\zeta} e^{-j2\pi m \frac{\tilde{f}_0}{\Delta f} \zeta + 2\pi k_2 \zeta} d\zeta \end{aligned}$$

and the constants

$$\begin{aligned} \Phi_2^{(l-)} &= \Phi_2(-\frac{1}{2}, 0, -1, -\nu_0 m \rho) & \Phi_3^{(l-)} &= \Phi_3(-\frac{1}{2}, 0, -1, -\nu_0 m \rho) \\ \Phi_2^{(l+)} &= \Phi_2(-\frac{1}{2}, 0, -1, \nu_0 m \rho) & \Phi_3^{(l+)} &= \Phi_3(-\frac{1}{2}, 0, -1, \nu_0 m \rho) \\ \Phi_2^{(r-)} &= \Phi_2(0, \frac{1}{2}, 1, -\nu_0 m \rho) & \Phi_3^{(r-)} &= \Phi_3(0, \frac{1}{2}, 1, -\nu_0 m \rho) \\ \Phi_2^{(r+)} &= \Phi_2(0, \frac{1}{2}, 1, \nu_0 m \rho) & \Phi_3^{(r+)} &= \Phi_3(0, \frac{1}{2}, 1, \nu_0 m \rho) \end{aligned}$$

one can derive

$$s s_H^{(l)}(\tau) = \begin{cases} \Phi_1(\tau; -\nu_0 m \rho, \Phi_2^{(l-)}, \Phi_3^{(l-)}), & \text{if } t < -\frac{1}{2} \\ \Phi_1(\tau; -\nu_0 m \rho, \Phi_2(\tau, 0, -1, -\nu_0 m \rho), \Phi_3(\tau, 0, -1, -\nu_0 m \rho)) + \\ \Phi_1(\tau; \nu_0 m \rho, \Phi_2(-\frac{1}{2}, \tau, -1, \nu_0 m \rho), \Phi_3(-\frac{1}{2}, \tau, -1, \nu_0 m \rho)), & \text{if } -\frac{1}{2} < \tau < 0 \\ \Phi_1(\tau; \nu_0 m \rho, \Phi_2^{(l+)}, \Phi_3^{(l+)}), & \text{if } \tau > 0 \end{cases}$$

$$s s_H^{(r)}(\tau) = \begin{cases} \Phi_1(t; -\nu_0 m \rho, \Phi_2^{(r-)}, \Phi_3^{(r-)}), & \text{if } \tau < 0; \\ \Phi_1(t; -\nu_0 m \rho, \Phi_2(\tau, \frac{1}{2}, 1, -\nu_0 m \rho), \Phi_3(\tau, \frac{1}{2}, 1, -\nu_0 m \rho)) + \\ \Phi_1(t; \nu_0 m \rho, \Phi_2(0, \tau, 1, \nu_0 m \rho), \Phi_3(0, t, 1, \nu_0 m \rho)), & \text{if } 0 < \tau < \frac{1}{2} \\ \Phi_1(t; \nu_0 m \rho, \Phi_2^{(r+)}, \Phi_3^{(r+)}), & \text{if } \tau > \frac{1}{2} \end{cases}$$

Note that both  $\Phi_2$  and  $\Phi_3$  can be rewritten in a closed but cumbersome form exploiting the error function definition in the complex domain.

Finally,  $\tilde{s}_N(\tau)$  is obtained by the periodic repetition of these functions as

$$\tilde{s}_N(\tau) = A_0 \frac{\pi \nu_0 m \rho}{2} \left( \sum_{k=-\infty}^{\infty} \tilde{s}s_N^{(l)}(\tau - k) + \sum_{k=-\infty}^{\infty} \tilde{s}s_N^{(r)}(\tau - k) \right) \quad (12)$$

## The two auxiliary functions

$$\Phi_4^-(\tau; k_2, \Phi_2, \Phi_3) = \sum_{k=-\infty}^{-1} \Phi_1(\tau-k, k_2, \Phi_2, \Phi_3) = \frac{e^{2\pi(j\frac{f_0}{\Delta f} - k_2)\tau}}{\left(e^{2\pi j\frac{f_0}{\Delta f}} - e^{2\pi k_2}\right)^2} \cdot e^{2\pi j\frac{f_0}{\Delta f}} \left( -e^{2\pi j\frac{f_0}{\Delta f}} (\Phi_2 + 2\pi k_2 \Phi_2 \tau + 2\pi k_2 \Phi_3) + e^{2\pi k_2} (\Phi_2 + 2\pi k_2 \Phi_2 (\tau + 1) + 2\pi k_2 \Phi_3) \right)$$

$$\Phi_4^+(\tau; k_2, \Phi_2, \Phi_3) = \sum_{k=1}^{\infty} \Phi_1(\tau-k, k_2, \Phi_2, \Phi_3) = \frac{e^{2\pi(j\frac{f_0}{\Delta f} - k_2)\tau}}{\left(e^{2\pi j\frac{f_0}{\Delta f}} - e^{2\pi k_2}\right)^2} \cdot e^{2\pi k_2} \left( e^{2\pi j\frac{f_0}{\Delta f}} (\Phi_2 + 2\pi k_2 \Phi_2 (\tau - 1) + 2\pi k_2 \Phi_3) + -e^{2\pi k_2} (\Phi_2 + 2\pi k_2 \Phi_2 \tau + 2\pi k_2 \Phi_3) \right)$$

are convergent if  $\Phi_2$  and  $\Phi_3$  are constant. Assuming without loss of generality that  $-1/2 < \tau < 1/2$  ( $\tilde{s}(t)$  and thus  $\tilde{s}_N(\tau)$  are periodic), we can split the sums in (12) such that

$$\tilde{s}_N(\tau) = A_0 \frac{\pi \nu_0 m \rho}{2} \left( \Phi_4^-(\tau; \nu_0 m \rho, \Phi_2^{(l+)}, \Phi_3^{(l+)}) + \tilde{s}_N^{(l)}(\tau) + \Phi_4^+(\tau; -\nu_0 m \rho, \Phi_2^{(l-)}, \Phi_3^{(l-)}) + \Phi_4^-(\tau; \nu_0 m \rho, \Phi_2^{(r+)}, \Phi_3^{(r+)}) + \tilde{s}_N^{(r)}(\tau) + \Phi_4^+(\tau; -\nu_0 m \rho, \Phi_2^{(r-)}, \Phi_3^{(r-)}) \right)$$

## REFERENCES

- [1] Code of Federal Regulations. Title 47 (47CFR), part 15, subpart B: "Unintentional Radiators", National Archives and Records Administration's Office.
- [2] "Council Directive on the approximation of the laws of the Member States relating to electromagnetic compatibility," Official Journal of the European Communities, No. L139/19, May, 23 1989, (89/336/EEC).
- [3] International Special Committee on Radio Interference (CISPR), "Specification for radio disturbance and immunity measuring apparatus and methods," Publication 16-1, 2004.
- [4] F. Mihalic and D. Kos, "Reduced Conductive EMI in Switched-Mode DC-DC Power Converters Without EMI Filters: PWM Versus Randomized PWM," *IEEE Transactions on Power Electronics*, vol. 21, no. 6, pp. 1783-1794, 2006.
- [5] M. Hartmann, H. Ertl, and J. Kolar, "EMI Filter Design for a 1 MHz, 10 kW Three-Phase/Level PWM Rectifier," *IEEE Transactions on Power Electronics*, vol. 26, no. 4, pp. 1192-1204, Apr. 2011.
- [6] L. Xing and J. Sun, "Conducted Common-Mode EMI Reduction by Impedance Balancing," *IEEE Transactions on Power Electronics*, vol. 27, no. 3, pp. 1084-1089, Mar. 2012.
- [7] K. B. Hardin, J. T. Fessler, and D. R. Bush, "Spread spectrum clock generation for the reduction of radiated emissions," in *IEEE International Symposium on Electromagnetic Compatibility*, Aug. 1994, pp. 227-231.
- [8] H. G. Skinner and K. P. Slattery, "Why spread spectrum clocking of computing devices is not cheating," in *2001 IEEE International Symposium on Electromagnetic Compatibility*, vol. 1, 2001, pp. 537-540.
- [9] M.-L. Yeh, W.-R. Liou, H.-P. Hsieh, and Y.-J. Lin, "An Electromagnetic Interference (EMI) Reduced High-Efficiency Switching Power Amplifier," *IEEE Transactions on Power Electronics*, vol. 25, no. 3, pp. 710-718, Mar. 2010.
- [10] X. Ming, Z. Chen, Z. kun Zhou, and B. Zhang, "An Advanced Spread Spectrum Architecture Using Pseudorandom Modulation to Improve EMI in Class D Amplifier," *IEEE Transactions on Power Electronics*, vol. 26, no. 2, pp. 638-646, Feb. 2011.
- [11] G. Setti, M. Balestra, and R. Rovatti, "Experimental verification of enhanced electromagnetic compatibility in chaotic FM clock signals," in *IEEE International Symposium on Circuits and Systems*, vol. 3, May 2000, pp. 229-232.
- [12] H.-H. Chang, I.-H. Hua, and S.-I. Liu, "A spread-spectrum clock generator with triangular modulation," *IEEE Journal of Solid-State Circuits*, vol. 38, no. 4, pp. 673 - 676, Apr. 2003.
- [13] K. B. Hardin, J. H. Fessler, D. R. Bush, and J. J. Booth, "Spread Spectrum Clock Generator and Associated Method," U.S. Patent 5 488 627, Jan. 30 1996.
- [14] "CY25561 Spread Spectrum Clock Generator," Cypress Semiconductor Corporation Document Number 38-07242, Mar. 2011. [Online]. Available: <http://www.cypress.com/?docID=9612>
- [15] "MB88155 Spread Spectrum Clock Generator," Fujitsu Microelectronics Data Sheet DS04-29119-2Ea, Nov. 2006. [Online]. Available: <http://www.fujitsu.com/downloads/MICRO/fma/pdf/e429119-2e.pdf>
- [16] S. Johnson and R. Zane, "Custom spectral shaping for EMI reduction in high-frequency inverters and ballasts," *IEEE Transactions on Power Electronics*, vol. 20, no. 6, pp. 1499-1505, Nov. 2005.
- [17] M.-W. Kim, D.-W. Kim, B.-S. Koo, Y.-B. Kim, O.-S. Choi, and N.-D. Kim, "Chip Level Techniques for EMI Reduction in LCD Panels," in *20th International Zurich Symposium on Electromagnetic Compatibility*, Jan. 2009, pp. 441-444.
- [18] Serial ATA International Organization, "Serial ATA Revision 2.6," Feb. 2007.
- [19] F. Pareschi, G. Setti, and R. Rovatti, "A 3-GHz Serial ATA Spread-Spectrum Clock Generator Employing a Chaotic PAM Modulation," *IEEE Transactions on Circuits and Systems-Part I: Regular Papers*, vol. 57, no. 10, pp. 2577-2587, Oct. 2010.
- [20] Y.-H. Kao and Y.-B. Hsieh, "A Low Power and High-Precision Spread Spectrum Clock Generator for Serial Advanced Technology Attachment applications Using Two-Point Modulation," *IEEE Transactions on Electromagnetic Compatibility*, vol. 51, no. 2, pp. 245-254, May 2009.
- [21] M. Kokubo et al., "A Low-Jitter Spread Spectrum Clock Generator Using FDM," *IEICE Transaction Electron*, vol. E89-C, no. 11, Nov. 2006.
- [22] Video Electronics Standards Associations, "VESA DisplayPort Standard Version 1," Jan. 2008.
- [23] "PCI Express Base Specification1," Mar. 2003, revision 1.1.
- [24] F. Lin and D. Y. Chen, "Reduction of power supply EMI emission by switching frequency modulation," *IEEE Transactions on Power Electronics*, vol. 9, no. 1, pp. 132-137, Jan. 1994.
- [25] J. Balcells, A. Santolaria, A. Orlandi, D. Gonzalez, and J. Gago, "EMI Reduction in Switched Power Converters using Frequency Modulation Techniques," *IEEE Transactions on Electromagnetic Compatibility*, vol. 47, no. 3, pp. 569-576, Aug. 2005.
- [26] D. Gonzalez et al., "Conducted EMI Reduction in Power Converters by Means of Periodic Switching Frequency Modulation," *IEEE Transactions on Power Electronics*, vol. 22, no. 6, pp. 2271-2281, Nov. 2007.
- [27] K. K. Tse, H. S.-H. Chung, S. Y. Huo, and H. C. So, "Analysis and spectral characteristics of a spread-spectrum technique for conducted EMI suppression," *IEEE Transactions on Power Electronics*, vol. 15, no. 2, pp. 399-410, Mar. 2000.
- [28] K. K. Tse, H. S.-H. Chung, S. Y. Ron Hui, and H. C. So, "A comparative study of carrier-frequency modulation techniques for conducted EMI suppression in PWM converters," *IEEE Transactions on Industrial Electronics*, vol. 49, no. 3, pp. 618-627, Jun. 2002.
- [29] K. Tse, R.-M. Ng, H.-H. Chung, and S. Hui, "An evaluation of the spectral characteristics of switching converters with chaotic carrier-frequency modulation," *IEEE Transactions on Industrial Electronics*, vol. 50, no. 1, pp. 171-182, Feb. 2003.
- [30] A. M. Stankovic, G. C. Verghese, and D. J. Perrault, "Analysis and synthesis of random modulation schemes for power converters," *IEEE Transactions on Power Electronics*, vol. 10, pp. 680-693, Nov. 1995.
- [31] A. Stankovic and H. Lev-Hari, "Randomized Modulation in Power Electronic Converters," *Proceedings of the IEEE*, vol. 90, no. 5, pp. 782-799, May 2002.
- [32] "LM5088 Evaluation Board," Texas Instruments Application Note 1913, Dec. 2008.
- [33] "P6P82PS01A: A "Drop-In" Active EMI Reduction IC For AC-DC and DC-DC Power Converters," ON Semiconductor Data Sheet, 2010. [Online]. Available: [http://www.onsemi.com/pub\\_link/Collateral/AND8477-D.PDF](http://www.onsemi.com/pub_link/Collateral/AND8477-D.PDF)
- [34] A. Santolaria, "Effects of Switching Frequency Modulation on the Power Converter's Output Voltage," *IEEE Transactions on Industrial Electronics*, vol. 56, no. 7, pp. 2729-2737, Jul. 2009.
- [35] H. S. Black, *Modulation Theory*. Van Nostrand, 1953.
- [36] "LTC6902 Multiphase Oscillator with Spread Spectrum Frequency Modulation," Linear Technology Data Sheet, 2003. [Online]. Available: <http://cds.linear.com/docs/Datasheet/6902f.pdf>
- [37] J. Proakis, *Digital Communications*, 4th ed. McGraw-Hill, Aug. 2000.
- [38] E. W. Weisstein, "Fresnel Integrals," From *MathWorld* - A Wolfram Web Resource. [Online]. Available: <http://mathworld.wolfram.com/FresnelIntegrals.html>
- [39] "Understanding Dynamic Signal Analysis," Agilent Application Note 1405-2, Aug. 2001.
- [40] "Spectrum Analysis Basics," Agilent Application Note 150, Jun. 2006.

- [41] "LM3424 Buck-Boost Evaluation Board," Texas Instruments Application Note 1967, Aug. 2009.



**Fabio Pareschi** (S'05-M'08) received the Dr.Eng. degree (with honors) in electronic engineering from University of Ferrara, Italy, in 2001, and the Ph.D. in Information Technology under the European Doctorate Project (EDITH) from University of Bologna, Italy, in 2007.

He is currently working as assistant professor in the Department of Engineering (ENDIF), University of Ferrara. He is also member of the Advanced Research Center on Electronic Systems (ARCES), University of Bologna. In 2006, he spent six months as a Visiting Scholar at the Department of Electrical Engineering of the Catholic University of Leuven, Belgium. Since 2010 he is serving as Associated Editor for the IEEE TRANSACTIONS ON CIRCUITS AND SYSTEMS—PART II.

His research activity is mainly focused on Analog and Mixed Mode electronic circuit design (in particular on non-linear and chaotic circuit implementation), statistical signal processing, random number generation and testing, and electromagnetic compatibility. He was co-recipient of the best paper award at ECCTD2005 and the best student paper award at EMCZurich2005.



**Gianluca Setti** (S'89-M'91-SM'02-F'06) received a Dr. Eng. degree (with honors) in Electronic Engineering and a Ph.D. degree in Electronic Engineering and Computer Science from the University of Bologna, Bologna in 1992 and in 1997, respectively, for his contribution to the study of neural networks and chaotic systems. From May 1994 to July 1995 he was with the Laboratory of Nonlinear Systems (LANOS) of the Swiss Federal Institute of Technology in Lausanne (EPFL) as visiting researcher. Since 1997 he has been with the School of Engineering at

the University of Ferrara, Italy, where he is currently a Professor of Circuit Theory and Analog Electronics. He held several visiting position at Visiting Professor/Scientist at EPFL (2002, 2005), UCSD (2004), IBM T. J. Watson Laboratories (2004, 2007) and at the University of Washington in Seattle (2008, 2010) and is also a permanent faculty member of ARCES, University of Bologna. His research interests include nonlinear circuits, recurrent neural networks, implementation and application of chaotic circuits and systems, statistical signal processing, electromagnetic compatibility, and compressive sensing.

Dr. Setti received the 1998 Caianiello prize for the best Italian Ph.D. thesis on Neural Networks. He is also recipient of the 2013 IEEE CAS Society Meritorious Service Award and co-recipient of the 2004 IEEE CAS Society Darlington Award, of the 2013 IEEE CAS Society Guillemin-Cauer Award, as well as of the best paper award at ECCTD2005, and the best student paper award at EMCZurich2005 and at ISCAS2011.

He served as an Associate Editor for the IEEE Transactions on Circuits and Systems - Part I (1999-2002 and 2002-2004) and for the IEEE Transactions on Circuits and Systems - Part II (2004-2007), the Deputy-Editor-in-Chief, for the IEEE Circuits and Systems Magazine (2004-2007) and as the Editor-in-Chief for the IEEE Transactions on Circuits and Systems - Part II (2006-2007) and of the IEEE Transactions on Circuits and Systems - Part I (2008-2009).

He was the 2004 Chair of the Technical Committee on Nonlinear Circuits and Systems of the of the IEEE CAS Society, a Distinguished Lecturer (2004-2005), a member of the Board of Governors (2005-2008), and he served as the 2010 President of the same society.

In 2012, he was the Chair of the IEEE Strategic Planning Committee of the Publication Services and Products Board (PSPB-SPC) and since 2013 is the first non North-American Vice President of the IEEE for Publication Services and Products.

Dr. Setti was the Track Chair for Nonlinear Circuits and Systems of ISCAS2004 (Vancouver), the Special Sessions Co-Chair of ISCAS2005 (Kobe) and ISCAS2006 (Kos), the Technical Program Co-Chair of NDES2000 (Catania), ISCAS2007 (New Orleans), ISCAS2008 (Seattle), ICECS2012 (Seville), BioCAS2013 (Rotterdam) as well as the General Co-Chair of NOLTA2006 (Bologna).

He is co-editor of the book *Chaotic Electronics in Telecommunications* (CRC Press, Boca Raton, 2000), *Circuits and Systems for Future Generation of Wireless Communications* (Springer, 2009) and *Design and Analysis of Biomolecular Circuits* (Springer, 2011), as well as one of the guest editors of the May 2002 special issue of the IEEE Proceedings on "Applications of Non-linear Dynamics to Electronic and Information Engineering".

He is a Fellow of the IEEE.



**Riccardo Rovatti** (M'99-SM'02-F'12) received the M.S. degree (summa cum laude) in electronic engineering and the Ph.D. degree in electronics, computer science, and telecommunications from the University of Bologna, Bologna, Italy, in 1992 and 1996, respectively. He is Full Professor of Electronics at the University of Bologna, Bologna, Italy.

He is the author of more than 300 technical contributions to international conferences and journals and of two volumes. He is coeditor of the book *Chaotic Electronics in Telecommunications* (CRC press, 2000) as well as one of the guest editors of the May 2002 special issue of the PROCEEDINGS OF THE IEEE on "Applications of Non-linear Dynamics to Electronic and Information Engineering." His research focuses on mathematical and applicative aspects of statistical signal processing especially those concerned with nonlinear dynamical systems.

Prof. Rovatti was an Associate Editor of the IEEE TRANSACTIONS ON CIRCUITS AND SYSTEMS-I: REGULAR PAPERS. In 2004, he received the Darlington Award and in 2012 he received the Guillemin-Cauer Award both from the IEEE Circuits and Systems Society.



**Giovanni Frattini** received the MS degree in electronic engineering (summa cum laude) from the University of Pavia, Italy, in 1997. The same year he joined STMicroelectronics in Milan, Italy, as an Analog Designer in the BCD technology R&D, where he worked on designing signal analog circuitry for smart power chips, data converters, HV linear and DC/DC power converters. In 2008 he joined National Semiconductor (which became part of Texas Instruments in 2011) to start and lead the R&D team in the Design Center in Milan, Italy, driving the development of chips for different applications, including photo-voltaics, ultrasound, LED driving, isolated power conversion, high frequency DC/DC converters.

He is author or co-author of 18 papers and he holds 13 patents.